Published in final edited form as:
Biomaterials. 2012 February ; 33(5): 1509–1519. doi:10.1016/j.biomaterials.2011.10.077.

ICP-MS Analysis of Lanthanide-Doped Nanoparticles as a Non-Radiative, Multiplex Approach to Quantify Biodistribution and Blood Clearance

Samuel H. Crayton[*], **Andrew Elias**[*], **Ajlan Al-Zaki**, **Zhiliang Cheng**, and **Andrew Tsourkas**[**]
Department of Bioengineering, School of Engineering and Applied Science, University of Pennsylvania, 210 S. 33rd Street, 240 Skirkanich Hall, Philadelphia, PA, 19104, USA

Abstract

Recent advances in material science and chemistry have led to the development of nanoparticles with diverse physicochemical properties, e.g. size, charge, shape, and surface chemistry. Evaluating which physicochemical properties are best for imaging and therapeutic studies is challenging not only because of the multitude of samples to evaluate, but also because of the large experimental variability associated with *in vivo* studies (e.g. differences in tumor size, injected dose, subject weight, etc.). To address this issue, we have developed a lanthanide-doped nanoparticle system and analytical method that allows for the quantitative comparison of multiple nanoparticle compositions simultaneously. Specifically, superparamagnetic iron oxide (SPIO) with a range of different sizes and charges were synthesized, each with a unique lanthanide dopant. Following the simultaneous injection of the various SPIO compositions into tumor-bearing mice, inductively coupled plasma mass spectroscopy (ICP-MS) was used to quantitatively and orthogonally assess the concentration of each SPIO composition in serial blood samples and the resected tumor and organs. The method proved generalizable to other nanoparticle platforms, including dendrimers, liposomes, and polymersomes. This approach provides a simple, cost-effective, and non-radiative method to quantitatively compare tumor localization, biodistribution, and blood clearance of more than 10 nanoparticle compositions simultaneously, removing subject-to-subject variability.

Keywords

Superparamagnetic iron oxide; Nanoparticle; ICP-MS; XPS; Biodistribution; clearance; multiplex

1. Introduction

Over the past decade, interest in the development of nanoparticles for clinical applications, such as diagnosis and drug delivery, has increased exponentially, along with the number of specific nanoparticle formulations reported in the literature [1–5]. Given the variety of nanomaterials from which they can be constructed, the array of physicochemical properties

[**]Corresponding Author: Dr. Andrew Tsourkas, 210 S. 33rd Street, 240 Skirkanich Hall, Philadelphia, PA 19104, Phone: 215-898-8167, Fax: 215-573-2071, atsourk@seas.upenn.edu.
[*]These authors contributed equally to this work

they can possess, and the assortment of specific molecular processes that can be targeted *in vivo*, the number of potential nanoparticle combinations is truly astronomical.

For most nanoparticle applications, a crucial research question is how much of the nanoparticle formulation (and thus imaging or therapeutic payload) reaches the tissue of interest. However, since determining this information directly and quantitatively is often impractical, indirect or semi-quantitative methods are usually employed. For example, relative nanoparticle delivery may be inferred from fluorescence intensity, imaging contrast, or alterations in tumor growth rate. However, since nanoparticle delivery is only one of several variables affecting fluorescence intensity, imaging contrast, and tumor growth rate, they cannot be assumed to represent nanoparticle delivery.

The “gold standard” for quantitative determination of biodistribution and blood clearance is through incorporation of a radioisotope within the compound of interest. Given the large number of radioisotopes to choose from, a compound can usually be radiolabeled by replacement of a stable isotope, ensuring the label has minimal impact on the behavior of the compound. Radiolabeling also has the advantage of being very sensitive. However, one major drawback to the use of radiolabeling is the special handling and containment protocols required when working with radioactivity. Therefore, a quantitative approach that does not require special laboratory precautions could make measurements of clearance and biodistribution more accessible.

Another, perhaps even more important, research question is how does one nanoparticle’s delivery to a tissue of interest compare to another’s. Whether comparing a new investigational agent to a negative control or optimizing a specific set of nanoparticles, such data are indispensable for development of better nanoparticle formulations and progression to clinical use. Beyond the difficulties of obtaining quantitative data for an individual nanoparticle’s biodistribution, there are also problems using this data to compare nanoparticle formulations due to the large experimental variability of *in vivo* studies. A convenient way to compare agents while controlling for subject-to-subject variability is to employ a ratiometric approach, whereby two or more agents are administered simultaneously to a single subject, and a “signal” from each one can be independently resolved. It is possible to employ a ratiometric approach with radiolabeling, using gamma emitters with resolvable energies [6] or a combination of gamma counting and scintillation [7], but physical limitations of energy resolution ultimately limit the number of compounds that can be simultaneously investigated.

In order to address these limitations, a method was designed that would allow for the quantitative determination of biodistribution and blood clearance of multiple nanoparticle formulations in single animal subjects using lanthanide metal tracers (Figure 1). Specifically, lanthanide metals were doped into the iron cores of superparamagnetic iron oxide (SPIO) nanoparticles, encapsulated within liposomes and polymersomes, and chelated to dendrimeric nanoparticles. Up to seven lanthanide-labeled nanoparticles were then injected in individual animals simultaneously. Inductively coupled mass spectrometry (ICP-MS) was then used to detect parts-per-billion (ppb) concentrations of lanthanide metals, independent of one another, in tissue and blood. Since lanthanide and other heavy metals (e.g. gold, silver, etc.) do not naturally exist within animal subjects, this “ICP-MS multiplex” approach provides a sensitive and straightforward method for quantitatively comparing the biodistribution and blood clearance of more than 10 nanoparticle formulations simultaneously, without the disadvantages of radioactivity and subject-to-subject variability. Notably, this method is intended to be restricted to pre-clinical animal studies, due to the possibility of long-term toxicity from lanthanide metal exposure.

2. Materials and Methods

2.1 Materials

Laboratory stock chemicals, as well as iron, lanthanide, and gold salts, were purchased from Sigma-Aldrich (St. Louis, MO, USA). Cell culture materials (medium, serum, trypsin and antibiotics) were purchased from Invitrogen (Carlsbad, CA, USA). All other materials were purchased as specified.

2.2 Synthesis of Dextran Stabilized Lanthanide Doped SPIO

Dextran coated, lanthanide doped, SPIO nanoparticles were prepared though the coprecipitation of ferrous, ferric, and lanthanide ions in the presence of dextran [8]. Briefly, 25 g of dextran T-10 (Pharmacosmos A/S, Holbaek, Denmark), was dissolved in 500 mL dH_2O and heated to 80°C for 1 hour. The solution was then allowed to cool to room temperature and continued to mix overnight. Subsequently, a solution of 1.85 g $FeCl_3$, 0.73 g $FeCl_2$, and 0.125 g $LnCl_3 \bullet 6H_2O$ (Ln = Ho, Eu, Er, Sm, or Gd) in 25 mL dH_2O was prepared and decanted into the dextran solution. The combined solution was cooled on ice and degassed with N_2 for 90 min. While keeping the solution stirring on ice and under N_2, an automated syringe pump was then used to introduce 15 mL of concentrated NH_4OH to the solution over 5 hours. The resulting black viscous solution was removed from the N_2 atmosphere, heated to 90°C for 1 hour, cooled overnight, and centrifuged at 20,000 RCF for 30 minutes to remove large aggregates. Free iron, lanthanide, and dextran were removed by diafilitration using a MidGee hoop cross flow cartridge with 100kDa molecular weight cutoff (GE Healthcare, Piscataway, NJ, USA) and the Ln-SPIO were brought to a final volume of ≈40 mL at 10 mg Fe/mL. The iron concentration of the SPIO solutions was determined by degrading and oxidizing an aliquot with hydrhloric acid and hydrogen peroxide and comparing optical absorbance measurements at 410 nm wavelength to a calibration curve, as described in [9].

This 40 mL of dextran SPIO at an iron concentration of 10 mg/mL was then combined with an equal volume of 10 M NaOH and mixed for 10 minutes. 80 mL of epichlorohydrin (Sigma-Aldrich, St. Louis, MO, USA) was then added and the solution was vigorously stirred at room temperature overnight. Epichlorohydrin crosslinks the dextran coating within the Ln-SPIO particle and chemically activates the dextran surface for conjugation. The solution was then briefly centrifuged to allow phase-separation into an aqueous black SPIO layer and a clear layer of unreacted epichlorohydrin, which was removed. The SPIO layer was quickly purified via extraction in isopropanol. Specifically, the Ln-SPIO material was combined with 5 volumes of isopropanol and the mixture was vigorously shaken. Brief centrifugation of the mixture resulted in a layer of precipitated salt, an Ln-SPIO layer, and an isopropanol layer (containing any remaining epichlorohydrin). The SPIO layer was then isolated and combined with an equal volume of concentrated NH_4OH and gently stirred for 24 hours at room temperature, resulting in an aminated nanoparticle surface. After the reaction, the Ln-SPIO was purified again by diafiltration on a 100kDa cutoff MidGee hoop and was filtered through a 0.2 μm nitrocellulose filter (Millipore, Billerica, MA, USA) to remove any oversized material. Finally, to ensure complete purification of the Ln-SPIO from excess salt and lanthanide ions, the nanoparticles were magnetically purified on MACS LS columns using a MidiMACS magnet (Miltenyi Biotec, Auburn, CA, USA).

To prepare SPIO with different surface charges, aminated Ln-SPIO formulations were reacted overnight with varying amounts of succinic anhydride (0 – 1 M) in 0.1 M sodium bicarbonate buffer and subsequently purified by isopropanol precipitation. Nanoparticles with distinct size distributions were obtained by differential centrifugation. Specifically, iterative centrifugation at 10,000 RCF for 10 minutes, resulted in a final nanoparticle pellet

enriched for larger sizes. Smaller nanoparticles were obtained by magnetic depletion (i.e. the flow-through of a MACS LS column was collected). Necessarily, this resulted in SPIO without magnetic properties, but selected for smaller nanoparticles, since particularly small iron cores do not have magnetic properties.

2.3 Synthesis of PAMAM (G3)–DOTA–Ho and PAMAM (G5)-DOTA-Pr

10 mg of PAMAM G3 dendrimer (ethylenediamine core, generation 3, Dendritech, Midland, MI, USA) was dissolved in 4 mL of sodium bicarbonate buffer (0.1 M, pH 9.5) and reacted with 35 mg of DOTA-NHS-ester (Macrocyclics, Dallas, TX, USA) for 10 hours. The pH of the solution was maintained at 9.5 over the course of the reaction by addition of NaOH. The PAMAM–DOTA was purified by centrifugal filter devices (Amicon Ultra-4, 5000 MWCO, Millipore, Billerica, MA, USA). The purified PAMAM–DOTA conjugates were mixed with 18 mg of $HoCl_3 \cdot 6H_2O$ in 0.1 M citrate buffer (pH 5.6) overnight at 42°C. Finally, the dendrimer was purified from free Ho^{3+} with 5000 MWCO centrifugal filter devices. PAMAM (G5)-DOTA- Pr was prepared using an analogous procedure, substituting PAMAM-G5 in the place of PAMAM-G3 and $PrCl_3 \cdot 6H_2O$ for $HoCl_3 \cdot 6H_2O$. In order to ensure the two dendrimer formulations were negatively charged, each was reacted overnight with 1 M succinic anhydride in 0.1 M sodium bicarbonate buffer and then purified by centrifugal filtration.

2.4 Preparation of DOTA–Ce Encapsulating Polymersomes

DOTA-Ce was prepared by dissolving 303 mg of DOTA (Macrocyclics) in 3 mL of citrate buffer (0.1 M, pH 5.6) and reacting with 223.8 mg of $CeCl_3 \cdot 7H_2O$ for 10 hours. The reaction solution was maintained at pH 6.0 with NaOH. Polymersomes were prepared by dissolving 20 mg of PEO-PBD block copolymer (polyethyleneoxide[600 Da]-*block*-polybutadiene[1200 Da], Polymer Source, Dorval, Quebec, Canada) in chloroform in a glass vial and then evaporating the solvent using a stream of N_2 gas. After further drying under vacuum overnight, the residual polymer film was hydrated with 1 mL DOTA-Ce aqueous solution in a 65 °C water bath for 30 min and then sonicated for another 1 h at the same temperature. Polymersomes were subjected to ten freeze–thaw–vortex cycles in liquid nitrogen and warm H_2O (65 °C), followed by extrusion 21 times through two stacked 100 nm Nuclepore polycarbonate filters using a stainless steel extruder (Avanti Polar Lipids, Alabaster, AL). Unencapsulated DOTA-Ce was removed via size-exclusion chromatography using Sepharose CL-4B (Sigma-Aldrich, St. Louis, MO, USA) and polymersomes were further purified through repeated washing on centrifugal filter devices (Amicon Ultra-4, 100K MWCO, Millipore).

2.5 Preparation of DOTA–Dy Encapsulating Liposomes

DOTA-Dy was prepared by dissolving 303 mg of DOTA in 3 mL of citrate buffer (0.1 M, pH 5.6) and reacting with 226.2 mg of $DyCl_3 \cdot 6H_2O$ for 10 hours. The reaction solution was maintained at pH 6.0 with NaOH. For liposome synthesis, hydrogenated soy phosphatidylcholine (HSPC), cholesterol, and 1,2-distearoyl-sn-glycero-3-phosphoethanolamine-N-[methoxy- (polyethylene glycol)-2000] (mPEG2000-DSPE) were obtained from Avanti Polar Lipids. 10 mg of 55 mol% HSPC/40 mol% CHOL/5 mol% mPEG2000-DSPE mixture was dissolved in chloroform in a glass vial, followed by evaporation of the solvent with a stream of N_2 gas and further drying under vacuum for at least 4 hours. DOTA-Dy encapsulating liposomes were then synthesized and purified with a procedure analogous to the preparation of DOTA-Ce encapsulating polymersomes.

2.6 Preparation of PEG-coated Gold Nanoparticles

Gold nanoparticles were prepared according to a protocol established by Turkevich [10]. Briefly, 200 ml of aqueous 0.01% (w/v) $HAuC1_4$ was brought to a boil and then 7 ml of aqueous 1% (w/v) sodium citrate was added. The color of the solution initially changed to a grayish-black and then to red within a few minutes. The solution was allowed to cool at room temperature and then filtered through a 0.2 μm pore size nylon filter system (Millipore). The AuNPs were then coordinated with HS – PEG (5K) – OCH_3 (Sigma Aldrich) at a mass ratio of 8:1 HS – PEG - OCH_3:Au. After 2 hours of constant stirring, the AuNP solution was then purified from excess reactants using 50K MWCO Amicon centrifugal filter devices.

2.7 Nanoparticle Physicochemical Characterization

Ln-SPIO stock samples were diluted in deionized water and deposited on 200-mesh carbon coated copper grids (Polysciences, Warrington, PA, USA) for TEM imaging with a JEOL 1010 transmission electron microscope operating at 80 kV. Mean iron core size was determined by measuring 100 individual nanoparticles. The presence of lanthanide metal incorporated into SPIO nanoparticles, versus the background solution, was assessed by energy dispersive X-ray spectroscopy (EDS) mapping using a JEOL 2010F. Stock samples of Ln-SPIO nanoparticles, dendrimers, polymersomes, and liposomes were diluted into pH 7.4 phosphate buffered saline for determination of the hydrodynamic diameter by dynamic light scattering (DLS). Measurements were acquired with a Zetasizer Nano-ZS (Malvern Instruments, Worcestershire, UK) using the non-invasive back-scatter (NIBS) mode. For zeta potential measurements, stock samples of Ln-SPIO, dendrimers, polymersomes, and liposomes were diluted into either 10 mM HEPES buffered water at pH 7.4 or phosphate buffered saline at pH 7.4 and then mean nanoparticle zeta potential was measured using a Zetasizer Nano-ZS. For Ln-SPIO nanoparticles, the transverse (r_2) and longitudinal (r_1) relaxivities were measured using a Bruker mq60 tabletop MR relaxometer operating at 1.41 T (60 MHz).

2.8 Nanoparticle Stability

The stability of the nanoparticles was measured as the amount of lanthanide leakage that could be observed in serum. Nanoparticles were incubated in 100% fetal bovine serum (FBS) at 37°C with shaking. Aliquots were removed at 1, 2, 4, 6, and 24 hours and applied to a 4,000 MWCO Amicon centrifugal filter device to collect any free metal in the filtrate. Lanthanide concentrations were measured by ICP-MS in the original nanoparticle stock and in the filtrates, allowing for calculation of percent of lanthanide leakage.

2.9 Cell Culture and Tumor Model

T6-17 murine fibroblasts (a derivative of the NIH/3T3 line and kindly provided by Mark Greene, PhD, FRCP, University of Pennsylvania) were cultured and maintained in Dulbecco's modified Eagle's medium (DMEM), supplemented with 10% fetal bovine serum (FBS), 1% penicillin/streptomycin at 37°C and 5% CO_2. Approximately 6-week old female nu/nu nude mice (Charles River Laboratory, Charles River, MA, USA) were maintained in accordance with the Institutional Animal Care and Use Committee of the University of Pennsylvania. Mice were anesthetized via isoflurane and T6-17 cells were injected subcutaneously into the back right flank (2×10^6 cells in 0.2 mL PBS). Tumors were grown until the longest dimension was approximately 8 mm.

2.10 Lanthanide-doped SPIO Cytotoxicity

The *in vitro* cytotoxicity of lanthanide-doped SPIO nanoparticles was assayed with an MTT cell viability kit (ATCC, Manassas, VA, USA). Specifically, T6-17 cells were seeded in 96-

well plates at a density of 10,000 cells per well. After overnight incubation (37°C and 5% CO_2), the medium in each well was removed and replaced with 100 μL of fresh medium containing 100 μg/mL of either Ho-SPIO, Eu-SPIO, Gd-SPIO, Sm-SPIO, or SPIO lacking any lanthanide dopant. After 24 hour incubation, the medium containing the nanoparticles was replaced with 100 μL fresh medium and 10 μL of MTT reagent. Following 2 hours of incubation, 100 μL of detergent reagent was added, and the plates incubated at room temperature in the dark overnight. The absorbance at 570 nm was then measured using a microplate reader (BioTek Instruments, Winooski, VT, USA).

2.11 Quantitation of Tumor Delivery, Biodistribution, and Blood Concentration by ICP- MS

Five animal cohorts, each containing 3 animals, were used for multiplex experiments, as outlined in Table 1. In the first 4 experimental groups, which investigated only SPIO nanoparticles, each nanoparticle formulation was injected at a dose of 10 mg Fe / kg body weight (for a total iron load of 10 mg/kg in group 1 and 30 mg/kg in groups 2–4). In the fifth experimental group, which investigated the addition of other nanoparticle platforms, the SPIO was injected at 10 mg Fe / kg body weight and the other formulations were injected at concentrations so that all tracer metal concentrations (lanthanide or gold) were approximately equal to that of the SPIO samples, ≈ 34 ppm, in 200 μL of injected solution.

For each experimental group, prior to injection, a nanoparticle aliquot was saved for inductively coupled plasma mass spectrometry (ICP-MS) determination of lanthanide concentration in the injected material. Following nanoparticle injection, 10 μL blood samples were collected from each animal, using the tail-nick method, at times of 1, 2, 4, 7, and 24 hours post-injection. After the final blood draw, the animals were sacrificed and the tumors, livers, spleens, kidneys, hearts, and lungs excised. Organ samples were thoroughly washed with phosphate-buffered saline (PBS) and blotted dry to minimize the contribution of any nanoparticles still circulating in the blood at 24 hours.

For ICP-MS analysis, analytical standards were purchased from SCP (Champlain, NY, USA) and trace metal grade nitric acid and aqua regia was purchased from Fisher Scientific (Pittsburg, PA, USA). All dilutions were done using in-house deionized water (≥18 MΩ-cm) obtained from a Millipore water purification system.

The pre-injection solutions, blood, tumor, and organ samples were analyzed for ^{158}Gd (gadolinium), ^{147}Sm (samarium), ^{153}Eu (europium), ^{165}Ho (holmium), ^{166}Er (erbium), ^{161}Dy (dysprosium), ^{140}Ce (cerium), ^{141}Pr (praseodymium), and ^{197}Au (gold) using an Elan 6100 ICP-MS (Perkin Elmer, Shelton, CT, USA) at the New Bolton Center Toxicology Laboratory, University of Pennsylvania, School of Veterinary Medicine, Kennett Square, PA, USA. The samples were weighed into Teflon PFA vials (Savillex, Minnetonka, MN, USA) and digested overnight with 70% nitric acid (or aqua regia for gold containing samples) at 70° C. 0.1 mL of 2 ppm ^{159}Tb (terbium) was added to each of the digested samples and the mixtures were diluted with deionized water to a final volume of 10 mL. The lanthanide (or gold) concentration of each sample was measured using a calibration curve of aqueous standards at 0.01, 0.1, 1.0, and 10 ppb for each metal.

The performance of the instrument and accuracy of the results were monitored by analyzing a reagent blank and bovine serum control serum (Sigma) prior to analysis of the samples. Also, standard reference material (Peach Leaves 1547) obtained from National Institute of Standards and Technology (NIST, Gaithersburg, MD, USA) with known values of iron and rare earth elements was analyzed with each batch of samples.

For each nanoparticle formulation, the percent injected dose per gram of tissue (% ID/g), was calculated as $[Ln]_{sample} / ([Ln]_{inj} * M_{inj})$ where $[Ln]_{sample}$ is the lanthanide concentration

in the sample (blood, tumor, or organ tissue), $[Ln]_{inj}$ is the lanthanide concentration in the injected nanoparticle solution, and M_{inj} is the mass of nanoparticle solution injected (0.2 grams).

3. Results

3.1 Synthesis of and Characterization of Ln-SPIO

Lanthanide doped superparamagnetic iron oxide (SPIO) nanoparticles were prepared by including a small amount of lanthanide metal with the ferric and ferrous salts during synthesis. Five different lanthanide metals (Gd, Eu, Ho, Sm, and Er) were successfully incorporated into SPIO nanoparticles. Following synthesis and purification of each Ln-SPIO formulation, differential centrifugation and chemical surface modification were used to generate orthogonal sets of nanoparticles having either fixed size and varying surface charge or fixed surface charge and varying size (Table 2). Specifically, to investigate the effect of surface charge, 6 nanoparticle formulations were generated, each with a hydrodynamic diameter of approximately 28 nm but with zeta potentials ranging from −20.8 mV to +14.3 mV (Figure 2A). Since it was hypothesized that negatively and positively charged nanoparticles could not be combined in a single injection due to electrostatic aggregation, these nanoparticles were divided into two sets, one with three negatively charged nanoparticles and one with 3 positively charged nanoparticles. Consequently, only three different Ln-SPIO cores were necessary (Gd, Eu, and Sm) for each of these studies. To investigate the effect of size, three nanoparticle formulations were generated, each with a zeta potential of approximately −20 mV, but with sizes of 15.52 nm, 29.05 nm, and 70.72 nm (Figure 2B). It should be noted that light scattering and zeta potential measurements were conducted in “clean” solutions (*e.g.* PBS) in order to ensure reproducible and accurate comparison between nanoparticle formulations. However, it is widely understood that, upon intravenous administration, a wide variety of blood plasma components may interact with nanoparticles leading to alterations in the “effective” values of size and charge of circulating nanoparticles [11].

The mean core size for each formulation of Ln-SPIO was determined by transmission electron microscopy (Table 2) and the core morphology was examined (Figure 3A-D). Consistent with SPIO previously synthesized by co-precipitation [8], the medium and large size formulations have cores consisting of multiple individual crystals, resulting in a heterogeneous appearance. Energy dispersive X-Ray spectroscopy (EDS) was used to further confirm that each lanthanide metal was incorporated into the iron core. Specifically, when examining the nanoparticles under transmission electron microscopy, EDS regions of interest placed in the background (i.e. not containing any nanoparticles) yielded signatures of ions of the buffer (Na, Cl) and the TEM grid itself (Cu), but no lanthanide was detectable in the background solution. When the EDS region of interest was moved onto a group of nanoparticles, very large Fe signatures were detected, as well as signatures corresponding to the specific lanthanide that was used for that synthesis (Figure 3E). EDS examination of conventional SPIO nanoparticles yielded only iron signatures without any lanthanide peaks.

MR imaging following a multiplex injection of SPIO nanoparticles provides little information, since the contribution of each individual nanoparticle formulation cannot be de-convoluted. Nevertheless, with the exception of Ho-SPIO, it was found that each Ln-SPIO nanoparticle used in the studies possessed magnetic relaxivities that were comparable to un-doped dextran SPIO (Table 2). The Ho-SPIO used in the size study had negligible magnetic relaxivity due to the method in which it was processed to obtain the small size. Prior to processing, the Ho-SPIO had relaxivities similar to the other Ln-SPIO formulations.

To ensure that the lanthanide metals within the core of each SPIO formulation would not readily leach/leak from the nanoparticle following intravenous injection, the stability of each Ln-SPIO was evaluated in serum (Supplemental Figure 1). Upon exposure to 100% serum for 24 hours at 37°C, each Ln-SPIO nanoparticle experienced less than 0.5% leakage of lanthanide metal into the bulk solution. In fact, for two of the Ln-SPIO (Sm and Eu) the amount of leakage was below the limit of detection (≈ 0.2%). Additionally, the in vitro cytotoxicity of Ln-SPIO was compared to nanoparticles lacking any lanthanide dopant (Supplemental Figure 2). Upon exposure to 100 μg/mL Ln-SPIO nanoparticles for 24 hours, the cell viability for every lanthanide remained greater than 90%, and no difference in cell viability was detectable between Ln-SPIO formulations and nanoparticles lacking lanthanide dopant (93.5% viability).

3.2 Effect of Surface Charge on SPIO Biodistribution

The surface charge of the nanoparticle (with a fixed hydrodynamic diameter of approximately 28 nm) was found to have a significant impact on passive tumor delivery (Figure 4A). Specifically, the mildly negative SPIO formulation (−12.2 mV in 10 mM HEPES) was found to have the highest tumor delivery at 2.05 % injected dose / gram tumor (% ID/g) 24 hours post-injection. Zeta potentials closer to neutrality (−5.2 mV and +3.6 mV) had somewhat lower tumor delivery of 1.37 and 1.23 % ID/g, while more extreme negative values (−20.8 mV) resulted in even less tumor delivery (1.09 % ID/g). The moderate and extreme positive values of zeta potential, at +10.0 mV and +14.3 mV, resulted in the poorest tumor delivery (0.84 and 0.29 % ID/g, respectively).

Nanoparticle accumulation in other organs (liver, spleen, kidney, lungs, and heart) was also examined 24 hours post-injection (Figure 4B). Large uptake was observed in organs of the reticuloendothelial system (RES), with liver concentrations ranging from 25–45 % ID/g and spleen concentrations ranging from 13–40 % ID/g. The lungs, kidney, and heart all showed modest uptake in the range of 0.5–2 % ID/g, with the notable exception of the heart delivery of the three positively charged SPIO nanoparticles. It was found that each positively charged SPIO had significantly elevated delivery to the heart, in the range of 5–7 % ID/g. These data were confirmed with a second set of mice. It was also found that at 5 minutes post-injection, the concentration of +14.3 mV SPIO nanoparticles in a washed heart specimen was 12.2 % ID/g, while its concentration in the blood at 5 minutes was only 2.3 % ID/g.

Finally, the blood clearance profile for each surface charge was investigated (Figure 4C). Similar to the results observed for tumor delivery, the −12.2 mV SPIO demonstrated the longest blood circulation time, while the more neutral formulations (−5.2 mV and +3.6 mV) had a shorter circulation time. The more positively charged particles exhibited very rapid clearance, with the +14.3 mV formulation’s blood concentration falling to 1.1 % ID/g in the first hour post-injection.

3.3 Effect of Nanoparticle Size on SPIO Biodistribution

The hydrodynamic diameter of SPIO nanoparticles (with a fixed zeta potential of approximately −20 mV) was also found to influence their passive tumor delivery (Figure 5A). Specifically, the smallest formulation of 15.52 nm yielded the greatest tumor delivery at 1.61 % ID/g, the medium sized formulation of 29.05 nm resulted in a lower delivery at 1.29 % ID/g, and the largest formulation of 70.72 nm demonstrated the lowest delivery at 1.06 % ID/g. Similarly to the negatively charged SPIO tested in the previous cohort of animals, all nanoparticle sizes demonstrated significant RES uptake (28 – 42 % ID/g in the liver and 18 – 38 % ID/g in the spleen) and more modest uptake in the heart, lungs, and kidneys (0.5 – 2 % ID/g, Figure 5B).

The blood clearance of the three different sizes tested proved especially interesting (Figure 5C). While the 29.05 nm, −20.7 mV nanoparticle exhibited a similar circulation profile as it did in the previous cohort of animals, both the smaller nanoparticle (15.52 nm) and the larger nanoparticle (70.72 nm) exhibited more prolonged circulation.

3.4 Generalization of ICP-MS Multiplex Method with Additional Nanoparticle Platforms

In order to demonstrate the generalizability and versatility of the ICP-MS multiplex approach, orthogonal metals were incorporated into a wide range of other nanoparticle platforms and their tumor delivery and blood clearance was examined. Specifically, the small molecule Gd-DTPA, PAMAM dendrimers of generation 3 and 5, PEG coated gold nanoparticles, SPIO, a polymersome, and a liposome were all synthesized and conjugated to or encapsulated with orthogonal metals (Table 3). This group of nanoparticles spanned a wide range of sizes, up to approximately 95 nm (Supplemental Figure 3). The stability of the dendrimer chelates and nanovesicle formulations was also confirmed by incubation in 100% serum for 24 hours at 37°C. It was found that less than 0.4% of the lanthanide metal was released from the dendrimer chelates into the bulk solution, and less than 1.5% of the lanthanide metal encapsulated within the liposome and polymersome was released into the bulk solution (Supplemental Figure 1).

These 7 formulations were simultaneously injected and their tumor delivery (Figure 6A) and blood clearance (Figure 6B) were evaluated. The small molecule Gd-DTPA and smallest particle (G3 dendrimer, 4.2 nm) had tumor delivery at or below the detection limit of 0.17% ID/g at 24 hours, and were entirely cleared from circulation in the first hour post-injection. Interestingly, the G5 dendrimer, with a size only slightly larger than the G3 dendrimer (6.1 nm) exhibited the greatest tumor delivery at 4.36% ID/g and a prolonged circulation time, with 5.83% ID/g still circulating at 24 hours post-injection. The significantly larger PEG-coated gold nanoparticle also demonstrated very robust tumor delivery at 4.00% ID/g and significantly lower clearance than any other formulation tested, with 15.20% ID/g remaining in circulation 24 hours post-injection. The SPIO nanoparticle had tumor delivery and blood circulation comparable to the previous studies. The polymersome and liposome yielded lower tumor delivery (0.35% ID/g and 1.00% ID/g, respectively), and correspondingly, faster blood clearance.

3.5 Validation of Multiplex Approach across Multiple Experimental Cohorts

A central assumption for all of the multiplex injection experiments was that the different nanoparticle formulations did not interact with each other, so that tumor delivery, biodistribution, and blood clearance observed in a multiplex injection are the same as they would be if each formulation were injected separately. The experimental cohorts used in this investigated were specifically designed to test and validate this assumption. A specific form of SPIO nanoparticle (≈ 30 nm hydrodynamic diameter and ≈ −20 mV zeta potential) was present in the multiplex injection of 3 different animal cohorts (negative zeta potential, size, and additional platforms), allowing for comparison of clearance and tumor delivery for this nanoparticle across a range of injection conditions. It should be noted that the zeta potential reported for the SPIO nanoparticle in Table 3 (−9.55 mV) was measured in isotonic phosphate buffered saline; zeta potential measured in 10 mM HEPES yielded ≈ −20 mV. Also, this formulation of SPIO was injected alone, in order to explicitly compare tumor delivery and clearance to the values obtained in the different multiplex injections.

The tumor delivery of this SPIO formulation conserved across animal cohorts is summarized in Figure 7A. For each injection condition tested, the tumor delivery was very similar (1.09 – 1.29 % ID/g), and no two conditions were statistically different (P values ranging from

0.33 to 0.85). Blood circulation profiles are compared in Figure 7B; again, the four injection conditions tested resulted in similar clearances, with overlapping error bars.

4. Discussion

4.1 Effect of Surface Charge on SPIO Clearance, Biodistribution, and Tumor Delivery—It should be noted that the absolute value of a zeta potential measurement is highly dependent on the identity and ionic strength of the buffer in which it is measured. The zeta potentials (as measured in pH 7.4, 10 mM HEPES, with no additional salt) of the 6 nanoparticle formulations tested in this investigation were −20.8, −12.2, −5.2, +3.6, +10.0, and +14.3 mV. A low ionic strength buffer was selected to measure zeta potential for this study in order to highlight relatively small differences in surface charge. In this buffer, the −5.2 mV and +3.6 mV formulations should be considered close to neutral; the −12.2 mV and +10.0 mV are mildly negative and positive, respectively; the remaining two formulations have more significant negative and positive charges.

Previous studies have demonstrated that prolonged blood circulation, and therefore, optimal tumor delivery by the enhanced permeability and retention (EPR) effect is achieved with nanoparticles displaying a neutral to mildly negative surface charge [12, 13]. When the surface charges becomes overly negative, excessive association with phagocytic cells of the reticuloendothelial system (RES) decreases circulation time [12, 13] and it has been commonly reported that positively charged nanoparticles are cleared very rapidly due to local electrostatic interactions near the injection site [14].

The results obtained in the two zeta potential experimental cohorts are consistent with this general literature consensus, and the tumor delivery was found to correlate well with blood circulation time, consistent with passive delivery by EPR. Specifically, the mildly negative surface charge of −12.2 mV yielded the longest circulation time and greatest tumor delivery. More neutral formulations resulted in slightly lower, but still significant, circulation time and tumor delivery. Excessively negative SPIO (−20.7 mV) displayed still more rapid clearance and decreased tumor delivery, while moderately and strongly positive formulations had poor circulation time and tumor delivery.

Unlike tumor delivery, uptake in other organs did not strongly correlate with nanoparticle circulation time. For organs such as the lungs, that do not play a major role in nanoparticle clearance or possess the leaky vasculature of tumors, a relatively low level of nanoparticle accumulation is observed regardless of blood circulation time.

As expected, a large amount of the injected material, for all surface charges, was found in the liver and spleen. However, the two surface charges that yielded the greatest tumor delivery (−5.2 mV and −12.2 mV) exhibited the least liver uptake. The more significantly negative formulation (−20.7 mV) had a larger liver uptake, consistent with stronger association with Kupffer cells and clearance by the liver. Given the liver's large mass and central role in nanoparticle clearance, combined with the fact that nanoparticles removed from circulation by the liver cannot end up delivered to the tumor, it was reasonable to observe the liver concentration as roughly inversely related to tumor delivery.

The relatively high concentration (≈ 6% ID/g) of positively charged nanoparticles observed in the heart 24 hours post-injection was an unexpected finding that is likely due to a "first pass effect", since the right chambers of the heart are the first organ that the nanoparticles reach after intravenous injection. In fact, washed heart tissue sampled at 5 minutes post-injection contained 12.2% ID/g. Since the nanoparticle concentration in the blood at 5 minutes post-injection was only 2.3% ID/g, the high concentration of nanoparticles detected in the heart cannot be attributed to residual blood in the chambers. The results are consistent

with a rapid initial interaction of the positively charged nanoparticles with the endocardium, followed by approximately half of this initial load being washed away during the next 24 hours. It is possible that investigators wishing to deliver nanoparticles to the endocardium could exploit this effect by infusing positively charged nanoparticles upstream of the chamber of interest (*e.g.* jugular vein cannulation for right heart delivery).

4.2 Effect of Hydrodynamic Diameter on SPIO Clearance, Biodistribution, and Tumor Delivery

Previous studies have shown that there is a window, roughly between 5 nm and 100 nm, in which nanoparticle blood circulation time and passive tumor delivery by EPR is maximized [15–18]. If the construct is too small, it can be rapidly and efficiently cleared through the kidneys, but if too large (>200 nm), it is efficiently trapped by cells of RES organs [19]. All three SPIO sizes tested were comfortably above the renal filtration threshold, so it was not surprising to observe an inverse relationship between nanoparticle size and tumor delivery.

However, unlike in the zeta potential studies, the tumor delivery was not observed to be strictly correlated to circulation time (the largest SPIO, at 70.72 nm, demonstrated the lowest tumor delivery, despite having intermediate circulation time). It is possible that the 70.72 nm SPIO exhibit greater blood concentrations (especially at early time points) because their larger size makes extravasation into tissue (including the tumor) more difficult, but the size is not yet large enough to result in excessive interaction with cells of the RES. It has also been demonstrated that diffusion-based penetration into tumors is strongly dependent on nanoparticle size [20]. It is likely the larger, 70.72 nm formulation, was not able to efficiently diffuse through the tumor tissue and, therefore, experienced a greater “wash out” effect over the 24 hours of the study.

4.3 Investigation of Additional Nanoparticle Platforms

The small molecule Gd-DTPA and the G3 dendrimer both had undetectable tumor delivery at 24 hours post-injection and had been cleared from circulation in the first hour post-injection. This is consistent with previous reports of G3 dendrimer’s rapid clearance [21]. Since both of these formulations are less than 5 nm in diameter, they are efficiently removed from circulation by renal filtration, and while they may display dynamic wash-in at the tumor site, their small size allows for efficient wash-out and, subsequently, poor tumor delivery at the 24 hour time point.

It has been reported that G5 dendrimer exhibits a significantly longer circulation time compared to G3 [22], as the G5 dendrimer’s small increase in size begins to impair renal filtration. In this study, the addition of the chelator DOTA, and surface modification with succinate (to neutralize the positive charge of a native PAMAM dendrimer) also contributes to increased size for the G5 formulation. The long circulation time observed in this study, and consequent high tumor delivery, was likely due to the formulation being too large for renal clearance, but still being small enough to avoid significant RES interaction.

The PEG-coated gold nanoparticle also exhibited very long circulation time and high tumor delivery. This was not unexpected since a PEG coating often confers “stealth” properties to nanoparticles [23] and many gold nanoparticle formulations have been reported to have relatively long circulation times [24]. The ≈ −20 mV, ≈ 30 nm SPIO demonstrated similar clearance and tumor delivery as it did in the previous experimental cohorts. Compared to the SPIO nanoparticles, the liposome and polymersome each displayed more rapid clearance and, consequently, lower tumor delivery.

4.4 Validation of Multiplex Approach across Experimental Cohorts

In order for the ICP-MS multiplex method to provide reliable data, it is important that the particular formulations that are co-injected together do not exhibit interactions with each other, so that in the co-injection they behave as they otherwise would if injected alone. In general, three potential sources of nanoparticle interaction should be considered: hydrophobic interactions, electrostatic interactions, and molecular specific interactions. For this particular investigation, all nanoparticle formulations possessed a significantly hydrophilic surface, and no nanoparticles possessed any specific ligands or receptors. In order to avoid electrostatic interactions, when the effect of nanoparticle surface charge was evaluated, the study was split into two separate injections (one with the three negatively charged particles, and one with the three positively charged particles). It is also worth noting that at no time, for any of the experimental groups, was any aggregation visibly observed when the individual formulations were combined to form the multiplex solution. Given that each nanoparticle would be “multivalent” for any possible type of interaction, macroscopic aggregation or precipitation would be expected if nanoparticle interaction had occurred.

As a way of confirming the assumption that the observed tumor delivery, biodistribution, and blood clearance was not affected by the presence of other nanoparticles in the co-injected solution, a specific SPIO nanoparticle formulation (≈ 30 nm hydrodynamic diameter and ≈ −20 mV zeta potential) was included in each experimental cohort and was also injected in isolation. It was found in all 4 cases that the blood clearance profiles overlapped and no statistical difference in tumor delivery was detected (Figure 7).

4.5 Improved Statistical Power of Multiplex (Ratiometric) Data

One of the most promising aspects of this multiplex ICP-MS approach to measuring biodistribution and blood clearance is the robust statistical power inherent in injecting all nanoparticle formulations one wishes to compare into a single animal. *In vivo* studies often exhibit a high degree of experimental variability (e.g. differences in tumor size, subject weight, and physiology). When each nanoparticle formulation is injected alone, comparison between formulations must be made with unpaired statistical tests, which often necessitates a larger number of animals in order to detect statistically significant differences in the performance of two or more nanoparticles. However, when each nanoparticle is simultaneously administered to all animals, subject-to-subject variability is effectively removed by the use of paired statistics. For example, the absolute tumor delivery of two particular nanoparticle formulations might be highly variable between three animals, confounding attempts to compare the formulations. However, if in each given subject, one nanoparticle is observed to have higher tumor delivery than the other, one can more easily conclude that formulation is superior.

Looking at the statistical analysis of the experimental cohort (3 animals) investigating the effect of nanoparticle size, between the 6 organs investigated for 3 sizes, there were 18 head-to-head statistical comparisons that could be made. Treating the data as unpaired, using $P < 0.05$ as the criterion, 6 of the comparisons were statistically significant; treating the data as paired, 15 of the possible 18 comparisons demonstrated statistical significance. To highlight a particular data set, the average kidney delivery of the 15.52 nm, 29.05 nm, and 70.72 nm sizes were 1.74, 1.29, and 1.16 % ID/g, respectively, each with a standard deviation of 0.26 – 0.29 % ID/g. These small differences in nanoparticle concentration could not be deemed statistically different (P values ranging from 0.06 to 0.59) from one another if the data are treated as unpaired. However, given that in a given animal, the 15.52 nm nanoparticle always had the greatest concentration, followed by 29.05 nm, and then 70.72 nm, paired statistics indicated that each concentration was statistically different (P values ranging from 0.002 to 0.022). However, it should not be assumed that paired statistics (compared to

unpaired) always necessarily result in a lower P value. In the experimental cohort investigating the effect of nanoparticle surface charge, there were several instances in which unpaired statistics would have produced P values less than 0.05 (which can always occur by chance when such a large number of comparisons are made) but paired analysis resulted in a P value greater than 0.05. The consequence of using paired statistics, therefore, is simply an increase in statistic power (i.e. a more accurate estimation of whether the difference is “real” can be obtained with a smaller sample size).

4.6 Future Applications of ICP-MS Multiplex Analysis

Perhaps more important than the specific results obtained in this investigation (i.e. the effect of size and charge on passive tumor delivery and biodistribution of nanoparticles), for a which a general consensus in the literature exists [12, 13, 25, 26], are the implications for future applications of the ICP-MS multiplex method. There are numerous physicochemical properties (e.g. size, shape, surface charge, surface chemistry, elasticity, and other mechanical properties) that can affect nanoparticle tumor delivery and biodistribution, all of which could be investigated using this method.

Additionally, the ICP-MS multiplex method could aid in the evaluation of the multitude of actively targeted nanoparticles under development. For example, negative control formulations can be simultaneously injected, allowing for convenient and accurate assessment of specificity *in vivo*. Also, the ICP-MS multiplex approach could be used to compare variations of a given actively targeted nanoparticle. For example, different ligand types, such as an antibody, single chain antibody fragment (scFv), or small affinity peptide could be quantitatively compared. Or, within a given class of ligand, different specific sequences could be compared (i.e. several affinity peptide sequences obtained from phage display). Since *in vivo* testing of each phage display hit individually would be costly and time consuming, most research groups usually select the highest affinity hit *in vitro* and then proceed to *in vivo* studies. However, it is possible for a lower affinity ligand to ultimately perform better *in vivo*, due to some predictable or unforeseen *in vivo* interaction [27, 28]. Therefore, the ICP-MS multiplex method could make it feasible for a greater number of formulations to be evaluated *in vivo*, facilitating the discovery of optimal nanoparticle formulations.

The ICP-MS multiplex approach could also be adapted to more specialized research questions. For example, nanoparticle trafficking and metabolism could be probed by labeling different components of the nanoparticle with different lanthanides (e.g. encapsulating one metal within a liposome core and chelating another metal to the lipid membrane component). Or chelation stability could be evaluated *in vivo* by constructing a given nanoparticle formulation but using different chelators to incorporate the metal. In general, it is envisioned the ICP-MS multiplex method could be exploited to answer any research question involving the *in vivo* comparison of two or more agents that are amenable to lanthanide labeling.

Furthermore, it is envisioned that the spatial distribution of each nanoparticle within an organ or other tissue sample could also be obtained with the use of laser ablation ICP-MS [29]. With LA-ICP-MS, the tissue sample is directly vaporized, layer-by-layer, with a pulsed laser and transported into the mass analyzer [30]. Another potential advantage of LA-ICPS-MS is the ability to process microgram samples sizes, which could be required for the analysis of smaller organs or specialized tissue (e.g. lymph nodes, adrenal glands).

4.7 Use of ICP-MS Multiplex Analysis to Generate Standardized Data

Another promising application of this multiplex ICP-MS method is the potential to generate standardized data that can be compared between studies and between laboratories. With so many research groups engaged in the development of nanoparticles, a myriad of different formulations have been synthesized for both imaging and therapeutic applications [31]. Even when nanoparticle (payload) delivery is quantitatively reported, it is difficult for one group to ascertain whether their formulation resulted in better tumor delivery than another's, given the numerous variables, known and unknown, involved in an *in vivo* study. This is a particularly significant problem in the nanoparticle field, and one that hinders the progress of nanoparticles into clinical evaluation [32]. However, if a rigorously standardized and highly reproducible lanthanide-doped nanoparticle (such as a G5 dendrimer with tightly chelated lanthanide) were available, each group could co-inject the standardized nanoparticle along with their investigational one. The delivery of the investigational agent could, therefore, be reported not only in absolute terms, but also as a ratio to the standardized particle. Such a ratiometric approach could facilitate accurate comparisons between various investigational agents.

5. Conclusion

A synthetic protocol to stably incorporate lanthanide metals into the core of SPIO nanoparticles, without abolishing their magnetic properties, has been developed. The lanthanide dopant can be used as a unique tracer atom, allowing the sensitive and quantitative detection of the nanoparticles by ICP-MS, both *in vitro* and *in vivo*, without interference from endogenous signals. When distinct lanthanide metals are incorporated into nanoparticles with distinct physicochemical properties, ICP-MS allows for the concentration of each nanoparticle formulation to be measured independently of other formulations that may be present in the solution or tissue of interest. As a proof of principle, this ICP-MS multiplex approach was used to evaluate the effect of nanoparticle size and surface charge on tumor delivery, biodistribution, and blood clearance *in vivo*. The results obtained were consistent with the general literature consensus about these properties and only required a small number of experimental animals, due to the inherent and robust statistical power of a multiplex (ratiometric) approach. The ICP-MS multiplex method was then extended to other nanoparticle formulations such as dendrimers, polymersomes, liposomes, and gold nanoparticles. Finally, it is envisioned that the ICP-MS multiplex analysis described could prove to be a powerful future research tool in the investigation of other nanoparticle formulations with diverse physicochemical properties and active targeting capabilities, while allowing for nanoparticle standardization.

Supplementary Material

Refer to Web version on PubMed Central for supplementary material.

Acknowledgments

This work was supported in part by the NIH (NCI/R21CA140695, NCI/R01CA157766, NIBIB/R01EB012065), the National Academies Keck Futures Initiative Imaging Science Grant, and the Department of Defense Breast Cancer Research Program (through a Predoctoral Traineeship Award given to SHC) W81XWH-10-1-0351. We would also like to thank Carol Buckley and Dr. Lisa Murphy of the University of Pennsylvania School of Veterinary Medicine for ICP-MS measurements.

References

1. Matson ML, Wilson LJ. Nanotechnology and MRI contrast enhancement. Future Med Chem. 2010; 2:491–502. [PubMed: 21426177]

2. Solomon M, D'Souza GG. Recent progress in the therapeutic applications of nanotechnology. Curr Opin Pediatr. 2011; 23:215–20. [PubMed: 21412081]
3. Tan SJ, Kiatwuthinon P, Roh YH, Kahn JS, Luo D. Engineering nanocarriers for siRNA delivery. Small. 2011; 7:841–56. [PubMed: 21374801]
4. Crayton, SH.; Chen, AK.; Cheng, Z.; Tsourkas, A. Molecular imaging. In: Ducheyne, P.; Healy, K.; Hutmacher, D.; Kirkpatrick, J., editors. Comprehensive biomaterials. Elsevier; 2011.
5. Thorek DL, Chen AK, Czupryna J, Tsourkas A. Superparamagnetic iron oxide nanoparticle probes for molecular imaging. Ann Biomed Eng. 2006; 34:23–38. [PubMed: 16496086]
6. Muzykantov VR, Puchnina EA, Atochina EN, Hiemish H, Slinkin MA, Meertsuk FE, et al. Endotoxin reduces specific pulmonary uptake of radiolabeled monoclonal antibody to angiotensin-converting enzyme. J Nucl Med. 1991; 32:453–60. [PubMed: 1848608]
7. Cahouet A, Denizot B, Hindre F, Passirani C, Heurtault B, Moreau M, et al. Biodistribution of dual radiolabeled lipidic nanocapsules in the rat using scintigraphy and gamma counting. Int J Pharm. 2002; 242:367–71. [PubMed: 12176281]
8. Thorek DL, Tsourkas A. Size, charge and concentration dependent uptake of iron oxide particles by non-phagocytic cells. Biomaterials. 2008; 29:3583–90. [PubMed: 18533252]
9. Moore A, Josephson L, Bhorade RM, Basilion JP, Weissleder R. Human transferrin receptor gene as a marker gene for MR imaging. Radiology. 2001; 221:244–50. [PubMed: 11568347]
10. Turkevich J, Stevenson PC, Hillier J. A study of the nucleation and growth processes in the synthesis of colloidal gold. Discuss Faraday Soc. 1951; 11:55–75.
11. Karmali PP, Simberg D. Interactions of nanoparticles with plasma proteins: implication on clearance and toxicity of drug delivery systems. Expert Opin Drug Deliv. 2011; 8:343–57. [PubMed: 21291354]
12. Moghimi SM, Davis SS. Innovations in avoiding particle clearance from blood by Kupffer cells: cause for reflection. Crit Rev Ther Drug Carrier Syst. 1994; 11:31–59. [PubMed: 7704918]
13. Moghimi SM, Hunter AC, Murray JC. Long-circulating and target-specific nanoparticles: theory to practice. Pharmacol Rev. 2001; 53:283–318. [PubMed: 11356986]
14. Chouly C, Pouliquen D, Lucet I, Jeune JJ, Jallet P. Development of superparamagnetic nanoparticles for MRI: effect of particle size, charge and surface nature on biodistribution. J Microencapsul. 1996; 13:245–55. [PubMed: 8860681]
15. Enochs WS, Harsh G, Hochberg F, Weissleder R. Improved delineation of human brain tumors on MR images using a long-circulating, superparamagnetic iron oxide agent. J Magn Reson Imaging. 1999; 9:228–32. [PubMed: 10077018]
16. Moore A, Marecos E, Bogdanov A Jr, Weissleder R. Tumoral distribution of long-circulating dextran-coated iron oxide nanoparticles in a rodent model. Radiology. 2000; 214:568–74. [PubMed: 10671613]
17. Zimmer C, Weissleder R, Poss K, Bogdanova A, Wright SC Jr, Enochs WS. MR imaging of phagocytosis in experimental gliomas. Radiology. 1995; 197:533–8. [PubMed: 7480707]
18. Zimmer C, Wright SC Jr, Engelhardt RT, Johnson GA, Kramm C, Breakefield XO, et al. Tumor cell endocytosis imaging facilitates delineation of the glioma-brain interface. Exp Neurol. 1997; 143:61–9. [PubMed: 9000446]
19. McNeil SE. Nanotechnology for the biologist. J Leukoc Biol. 2005; 78:585–94. [PubMed: 15923216]
20. Perrault SD, Walkey C, Jennings T, Fischer HC, Chan WC. Mediating tumor targeting efficiency of nanoparticles through design. Nano Lett. 2009; 9:1909–15. [PubMed: 19344179]
21. Kobayashi H, Kawamoto S, Jo SK, Bryant HL Jr, Brechbiel MW, Star RA. Macromolecular MRI contrast agents with small dendrimers: pharmacokinetic differences between sizes and cores. Bioconjug Chem. 2003; 14:388–94. [PubMed: 12643749]
22. Sato N, Kobayashi H, Hiraga A, Saga T, Togashi K, Konishi J, et al. Pharmacokinetics and enhancement patterns of macromolecular MR contrast agents with various sizes of polyamidoamine dendrimer cores. Magn Reson Med. 2001; 46:1169–73. [PubMed: 11746584]
23. Jokerst JV, Lobovkina T, Zare RN, Gambhir SS. Nanoparticle PEGylation for imaging and therapy. Nanomedicine (Lond). 2011; 6:715–28. [PubMed: 21718180]

24. De Jong WH, Hagens WI, Krystek P, Burger MC, Sips AJ, Geertsma RE. Particle size-dependent organ distribution of gold nanoparticles after intravenous administration. Biomaterials. 2008; 29:1912–9. [PubMed: 18242692]

25. Poznansky MJ, Juliano RL. Biological approaches to the controlled delivery of drugs: a critical review. Pharmacol Rev. 1984; 36:277–336. [PubMed: 6395142]

26. Tomalia DA, Reyna LA, Svenson S. Dendrimers as multi-purpose nanodevices for oncology drug delivery and diagnostic imaging. Biochem Soc Trans. 2007; 35:61–7. [PubMed: 17233602]

27. Aggarwal P, Hall JB, McLeland CB, Dobrovolskaia MA, McNeil SE. Nanoparticle interaction with plasma proteins as it relates to particle biodistribution, biocompatibility and therapeutic efficacy. Adv Drug Deliv Rev. 2009; 61:428–37. [PubMed: 19376175]

28. Huang RB, Mocherla S, Heslinga MJ, Charoenphol P, Eniola-Adefeso O. Dynamic and cellular interactions of nanoparticles in vascular-targeted drug delivery. Mol Membr Biol. 2010; 27:312–27. [PubMed: 21028938]

29. Hsieh YK, Jiang PS, Yang BS, Sun TY, Peng HH, Wang CF. Using laser ablation/inductively coupled plasma mass spectrometry to bioimage multiple elements in mouse tumors after hyperthermia. Anal Bioanal Chem. 2011; 401:909–15. [PubMed: 21667060]

30. Koch J, Gunther D. Review of the state-of-the-art of laser ablation inductively coupled plasma mass spectrometry. Appl Spectrosc. 2011; 65:155–62. [PubMed: 21513587]

31. Jain KK. Advances in the field of nanooncology. BMC Med. 2010; 8:83. [PubMed: 21144040]

32. Stark WJ. Nanoparticles in biological systems. Angew Chem Int Ed Engl. 2011; 50:1242–58. [PubMed: 21290491]

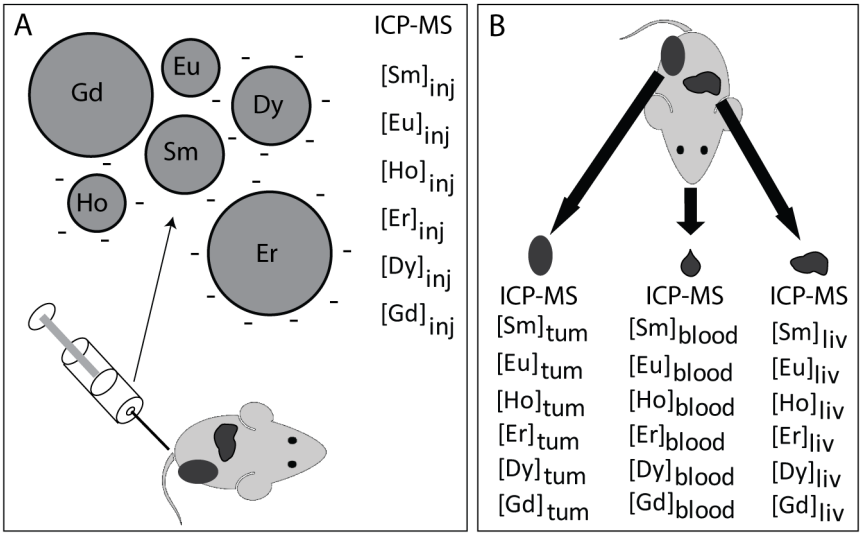

Figure 1.

Schematic of the ICP-MS based multiplex method for determining biodistribution and blood clearance. (A) Nanoparticles of varying physicochemical properties are combined into a single solution. Each type of nanoparticle is associated with a unique lanthanide metal; either by encapsulation or chelation (for example, the large and neutral particle contains Gd while the small and negative particle contains Ho). The concentration of each lanthanide metal in the injected solution is measured by ICP-MS and the combined solution is injected intravenously into the animal. (B) Blood samples are drawn at various times post-injection and following the final blood draw, the animal is sacrificed and the tumor and other organs are excised and rinsed in water. The blood and tissue samples are weighed and digested with nitric acid, and then the concentration of each lanthanide metal is determined by ICP-MS.

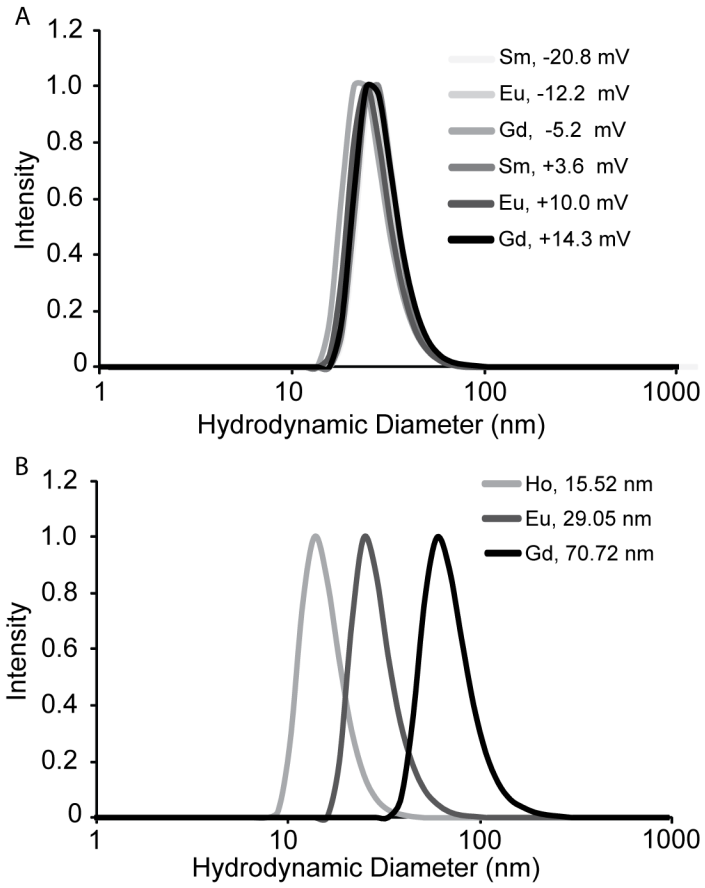

Figure 2.

Dynamic light scattering (DLS) size distributions for Ln-SPIO nanoparticles. (A) The six nanoparticle formulations used to investigate the effect of zeta potential on nanoparticle biodistribution and blood clearance have near-equivalent size distributions. (B) The three nanoparticle formulations that were used to isolate the effect of size on nanoparticle biodistribution and blood clearance have distinct size distributions (each with zeta potential ≈ -20 mV).

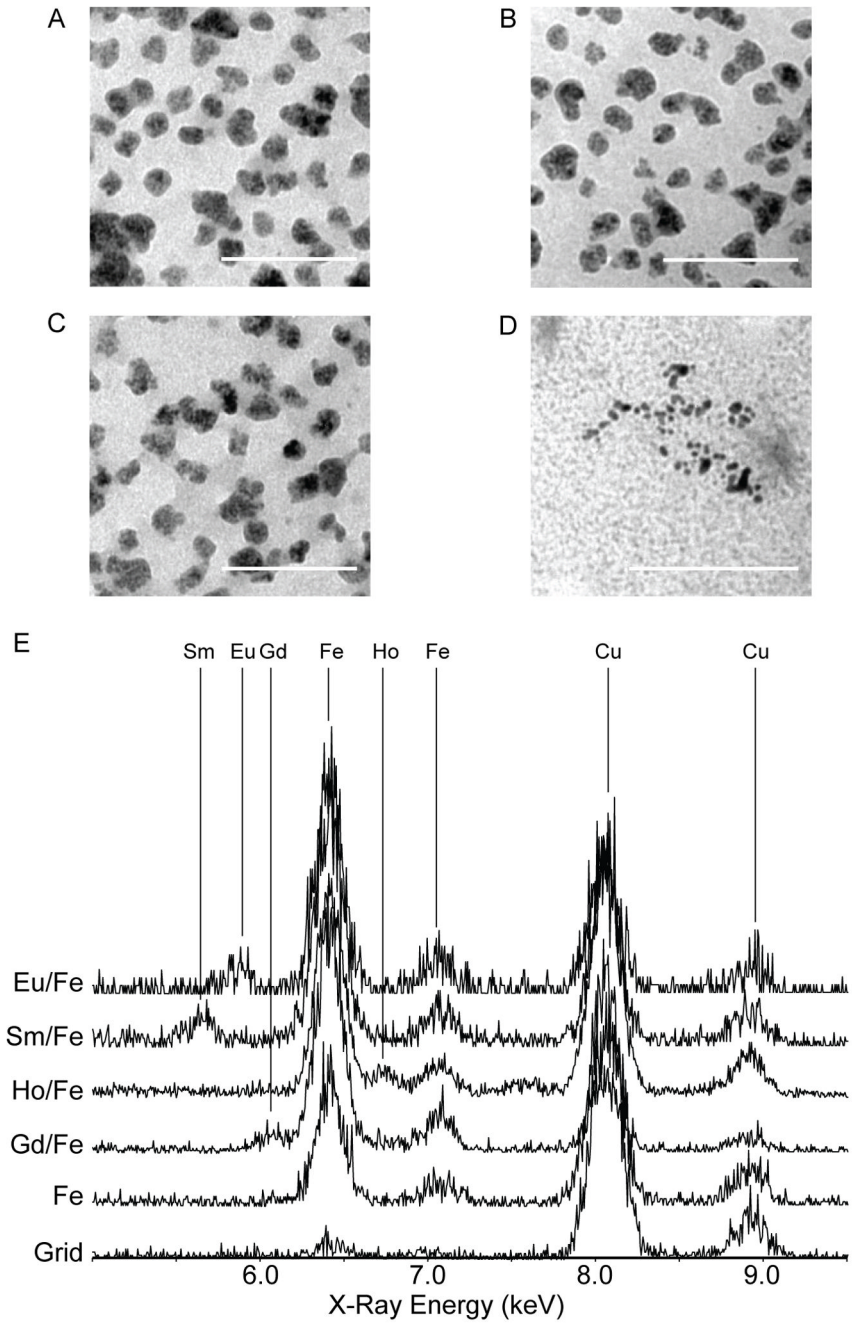

Figure 3.

TEM images and EDS profiles of Ln-SPIO. Representative TEM images of (A) Sm-SPIO (core size, CS = 19.4±3.9nm, hydrodynamic diameter, HD = 29.84nm), (B) Eu-SPIO (CS = 19.2±3.5nm, HD = 28.61nm), (C) Gd-SPIO (CS = 15.9±2.7nm, HD = 26.06nm) and (D) Ho- SPIO (CS = 5.1±1.9nm, HD = 15.52nm). All scale bars are 100 nm. (E) EDS spectra of background (Grid), iron only SPIO (Fe), and Ln-SPIO doped with either Eu, Sm, Ho, or Gd, demonstrating specific incorporation of each lanthanide metal into the nanoparticle core.

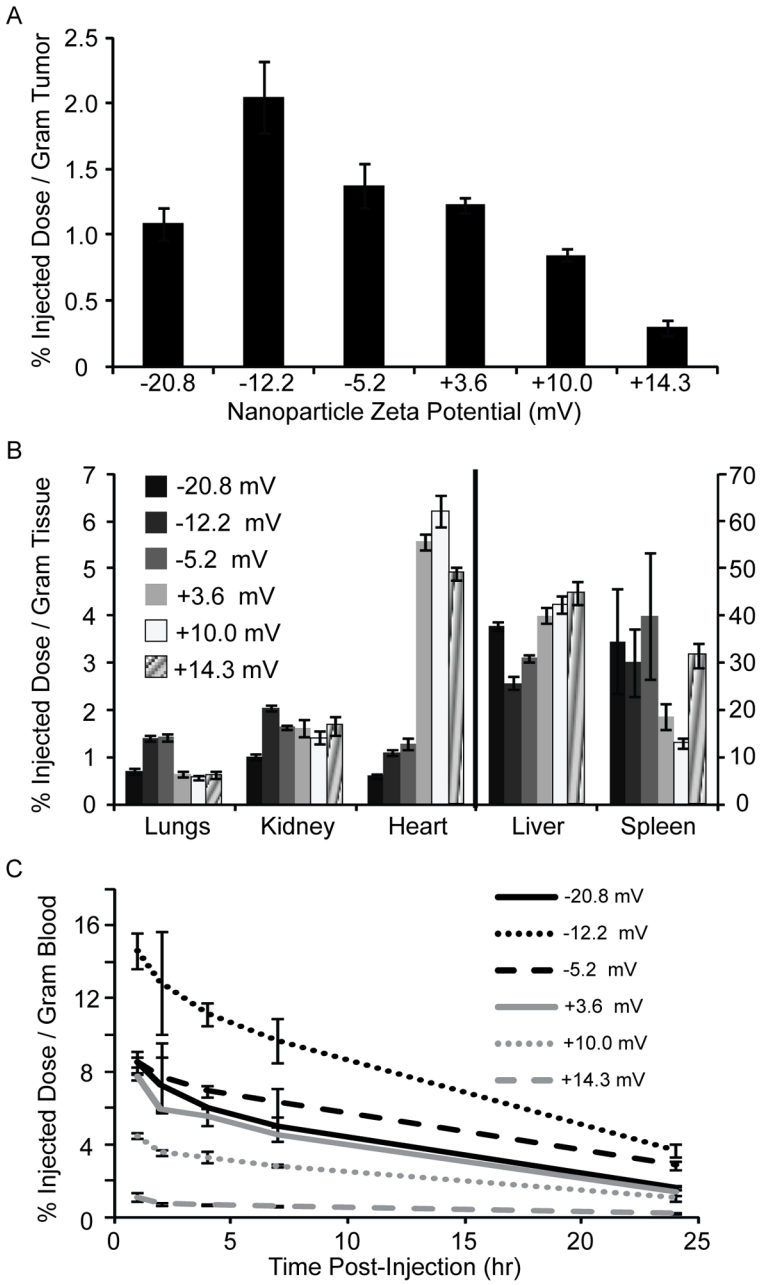

Figure 4.

Effect of SPIO surface charge on biodistribution, at 24 hours post-injection, and blood clearance. (A) Passive nanoparticle delivery to a flank tumor (percent injected dose per gram tumor) as a function of nanoparticle surface charge. (B) Nanoparticle uptake in other organs as a function of surface charge. (C) Blood clearance profiles of each nanoparticle investigated.

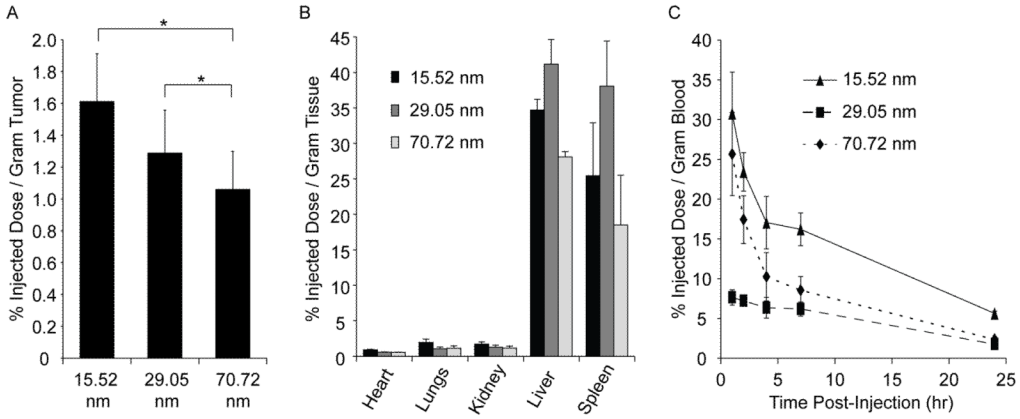

Figure 5.

Effect of SPIO hydrodynamic diameter on biodistribution and blood clearance. (A) Passive nanoparticle delivery to a flank tumor for three distinct SPIO size distributions. (B) Nanoparticle uptake in other organs as a function of size. (C) Blood clearance profiles of each size investigated.

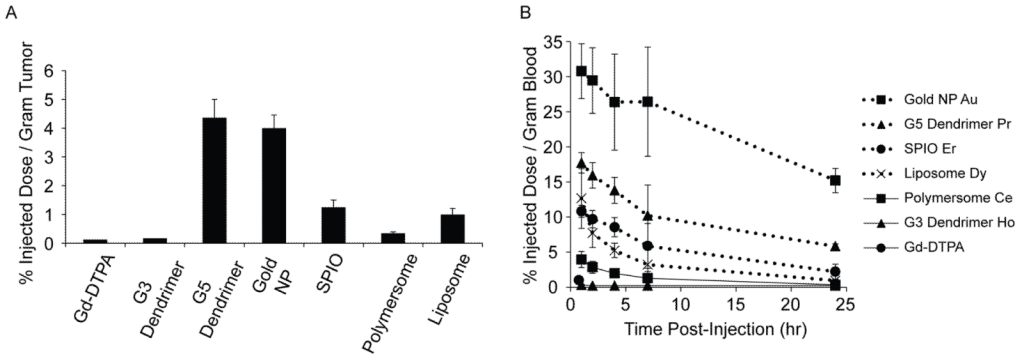

Figure 6.

ICP-MS multiplex analysis of biodistribution and blood clearance for seven different compounds injected simultaneously. (A) Tumor delivery and (B) blood clearance profiles for a variety of lanthanide doped nanoparticle formulations, spanning a range of sizes, including small molecules, dendrimers, gold nanoparticles, SPIO nanoparticles, polymersomes, and liposomes.

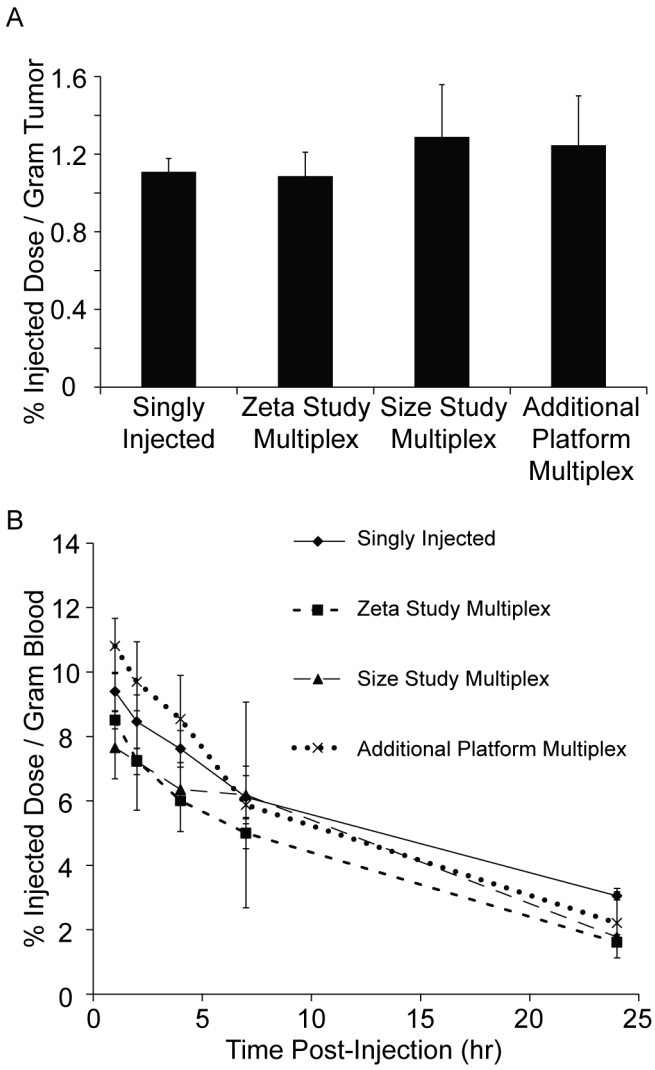

Figure 7.

Validation of the ICP-MS multiplex method by comparing tumor delivery and blood clearance of a single SPIO nanoparticle formulation (≈ 29 nm, ≈ −20 mV) that was injected across multiple studies. (A) No statistical difference is found between tumor delivery obtained when the same SPIO formulation is injected alone, with SPIO of other charges, with SPIO of other sizes, or with various other nanoparticle platforms. (B) Blood clearance of the same SPIO formulation is also very similar across the various studies.

Table 1

Summary of animal injection groups (n=3 for all groups).

Experimental Cohort	Number of Particles Co-injected	Description
Single Particle	1	−20.8 mV, 29.8 nm SPIO
Negative Zeta Potential	3	−20.8 mV, −12.2 mV, −5.2 mV SPIO (all ≈ 28 nm)
Positive Zeta Potential	3	+3.6 mV, +10.0 mV, +14.3 mV SPIO (all ≈ 28 nm)
Size	3	15.52 nm, 29.05 nm, 70.72 nm SPIO (all ≈ −20 mV)
Additional Platforms	7	Gd-DTPA, G3 and G5 dendrimers, AuNP, SPIO, liposome, polymersome

Table 2

Physicochemical properties of the nine unique Ln-SPIO formulations.

Tracer Metal	Hydrodynamic Diameter (nm)	Zeta Potential (mV), HEPES, pH 7.4	r2 ($mM^{-1}s^{-1}$)	r1 ($mM^{-1}s^{-1}$)	Core Size (nm)	Ln / Fe%
Ho	**15.52**	−19.6	< 5	< 0.5	5.1 ± 1.9	17.8
Eu	**29.05**	−20.7	141.75	9.35	17.4 ± 3.0	1.6
Gd	**70.72**	−19.6	214.97	2.26	41.1 ± 10.6	8.0
Sm	29.84	**−20.8**	150.41	9.99	19.4 ± 3.9	1.7
Eu	28.61	**−12.2**	137.18	9.10	19.2 ± 3.5	2.9
Gd	26.06	**−5.2**	123.66	11.79	15.9 ± 2.7	2.0
Sm	29.16	**+3.6**	142.38	9.22	19.8 ± 3.8	1.7
Gd	27.29	**+10.0**	106.76	10.31	15.1 ± 2.6	2.0
Eu	29.47	**+14.3**	176.58	8.87	18.6 ± 3.8	2.9

Table 3

Size and zeta potential of the nanoparticles used in the multiplatform study.

Particle	Tracer Metal	Hydrodynamic Diameter (nm)	Zeta Potential (mV), PBS, pH 7.4
Gd-DTPA	Gd	--	--
G3 Dendrimer	Ho	4.2	−0.38
G5 Dendrimer	Pr	6.1	−7.58
Gold NP	Au	26.0	−1.31
SPIO	Er	33.3	−9.55
Polymersome	Ce	82.5	−4.08
Liposome	Dy	93.8	−1.35